Session E VIII.1 Version 1. Completed 5/28/96

Observations of alloying in the growth of Cr on Fe(001)

A. Davies, Joseph A. Stroscio, D. T. Pierce, J. Unguris, and R. J. Celotta

Electron Physics Group
National Institute of Standards and Technology
Gaithersburg, Maryland 20899

Abstract

Using scanning tunneling microscopy, we observe the alloying of Cr with an Fe(001) substrate for various coverages at two temperatures. At low Cr coverage, the alloy consists of individual Cr impurities surrounded by Fe. Elemental identification is possible using surface states observed via tunneling spectroscopy. The alloy may be the cause of several magnetic anomalies observed in Cr/Fe structures.

Keywords: scanning tunneling microscopy, scanning tunneling spectroscopy, Fe, Cr, alloy, magnetic multilayers.

Corresponding Author: A. Davies, NIST, Bldg. 220 Rm. B206, Gaithersburg, MD 20899. Phone (301) 975-3521. FAX (301) 926-2746. e-mail: davies@epg.nist.gov

The properties of magnetic multilayers can be strongly affected by the structure of their interfaces. The study of exchange coupling in epitaxial Fe/Cr/Fe provides a good example. Fe/Cr/Fe is a particularly good system in which to compare experiment to theory because nearly ideal layer structures can be grown, due to the low lattice mismatch (< 0.6 %) and the availability of ultra-flat Fe whisker substrates. Such structures have revealed more than 70 alignment reversals in the coupling of Fe layers with increasing Cr thickness [1]. Scanning electron microcopy with polarization analysis (SEMPA) and scanning tunneling microscopy (STM) measurements of this system have shown the strong effect of intralayer thickness fluctuations on the relative strengths of coupling oscillations of different periods[2].

Although we know a great deal about the magnetism in the Fe/Cr system, some aspects are still not understood. For example, in Fe/Cr/Fe sandwich structures the phase of the exchange coupling for thin Cr intralayers is opposite to what is expected based on simple models of antiferromagnetic coupling. With antiferromagnetic stacking of the Cr layers and antiparallel coupling between Cr and Fe as shown by photoemission measurements [3], two Fe layers separated by an *odd* number of Cr layers are expected to align ferromagnetically. But, both SEMPA [1] and Brillouin light scattering [4] measurements find that at low interlayer thicknesses, *even* numbers of Cr layers give rise to ferromagnetic coupling. A SEMPA measurement of the exchange coupling in Fe/Cr/Fe is shown at the bottom of Figure 1.

Anomalies are seen in surface magnetization measurements of bare Cr on Fe(001). A SEMPA measurement of a Cr wedge grown at 300 °C on an Fe(001) whisker is shown in the

top of Figure 1 [5]. The horizontal axis represents position along the Cr wedge, which has been converted to the average thickness of the Cr at each position. The vertical axis is the spin polarization of secondary electrons after an exponential fit has been subtracted to approximately remove the contribution from the underlying Fe substrate. Positive values indicate a polarization which is parallel to the Fe magnetization. There are several surprising aspects of the remaining polarization signal. First, the two-layer-period oscillation from the antiferromagnetic ordering of the Cr overlayer is present; however, strong oscillations do not set in until a Cr coverage of ~3 monolayers (ML). Second, maxima in the polarization are present for *odd* layers of Cr. Again, this is opposite to what we expect, assuming antiferromagnetic coupling between Cr and Fe [3]. Finally, the surface polarization changes abruptly for Cr coverages up to ~0.2 ML, as shown in the inset in the figure. While the exact shape and magnitude of this polarization feature depend on the details of the background subtraction, the same type of feature has been observed in many experiments with different Fe(001) whiskers. The polarization of the electrons responsible for the feature is likely much larger than the values shown in the plot because these electrons are probably emitted from only a fraction of a monolayer.

Similar anomalies are observed in other measurements of Cr growth on Fe. An initial rapid decrease in the average surface moment is also observed in recent alternating gradient magnetometer measurements [6]. The delay in the onset of clear antiferromagnetic ordering is seen in inelastic polarized electron scattering measurements[7], but unlike the SEMPA results, odd layers of Cr are found to align antiparallel to the Fe substrate magnetization.

Using scanning tunneling microscopy (STM) to investigate growth of Cr on Fe(001) we have identified the formation of a Cr/Fe alloy that may be the cause of the anomalies [8]. We show that submonolayer deposition of Cr on Fe(001) results in the formation of an alloyed substrate and growth layer, both of which consist of low concentrations of isolated Cr impurities surrounded by Fe. We distinguish Cr atoms from Fe atoms in the surface by observing the spatial variation of an Fe(001) surface state. The surface state gives rise to a unique tunneling conductance peak observed near the Fermi energy. For low Cr coverages, where alloyed Cr atoms can be individually identified in the STM images, we quantitatively evaluate both the spatial distribution and the average concentration.

The experiments are performed in an ultra-high vacuum system with thin film growth, reflection high-energy electron diffraction, and room-temperature STM capabilities, as previously described [9]. We use single-crystal Fe(001) whisker substrates[10] and deposit Cr at a rate of approximately 0.8 monolayers per minute.

An STM image of ~0.4 monolayers of Cr deposited on an Fe(001) whisker is shown in Figure 2. The Cr is deposited at 290 ± 10 °C, under layer-by-layer growth conditions as indicated by the presence of only single atomic-step islands. The area of the islands is used to estimate the coverage. The islands tend to facet along <100> directions as happens in Fe homoepitaxial growth [11]. A higher-resolution image of the surface is shown in Figure 2 (b) where the upper terraces are the 0.14 nm-high islands resulting from the growth. On this scale, we see 0.01 nm features on both the substrate and island levels which indicate a chemical nonuniformity.

The lateral scale and uniformity of the features can be seen more clearly in the top-view shown in Figure 3 (a). Separate gray-scales are used for each terrace to display the small vertical variations. The white dots on both substrate (the central region) and island (regions surrounded by heavy black lines) levels are all ~0.5 nm wide (full-width half maximum). The height contrast of the features is at most 0.01 nm and is voltage-dependent; the contrast is positive (negative) when imaging the filled (empty) states of the sample. The irregular dark features are also seen in images of nominally clean Fe whiskers and are probably due to contamination from residual gases in the chamber. The uniformity, size, and voltage-dependence of the white-dots suggests that each feature is a single substitutional impurity atom in the surface layer, indicating the presence of a Cr/Fe surface alloy.

To confirm this interpretation, we identify Fe regions of the surface through the presence of an Fe(001) surface state. As shown in Figure 4, this surface state gives rise to a sharp conductance peak at a sample voltage of +0.17 V. The surface state is a general property of transition metal bcc(001) surfaces, resulting in a similar sharp conductance peak on Cr(001) (see Figure 4) [12]. The solid-line curves in Figure 4 are representative of spectra on the alloyed surface. A strong conductance peak at the Fe surface state voltage is present when the tip is away from the impurity features and over the smooth grey regions in the images. We then identify these regions as Fe and conclude that the dot-like features are substitutional Cr atoms. Over the Cr impurities, the Fe surface state conductance peak is attenuated and an additional peak is present in the filled states. The Fe surface state is also present in the smooth gray regions on the islands, indicating that the growth layer is also an

Fe-rich Fe/Cr alloy, as shown in the schematic at the bottom of Figure 4.

At low coverages, where all of the Cr impurities can be identified, we can quantify both the spatial distribution of the Cr impurities and the surface Cr concentration from the STM images. The spatial correlation is determined from the two-dimensional pair distribution function. Relative Cr-pair coordinates are extracted from the high resolution STM image shown in Figure 5 (a), and these coordinates are plotted in Figure 5 (b). Multiple occurrences (within some bin size) are indicated by proportionately increasing the area of the symbol plotted. The horizontal and vertical axes of the plot are aligned with the <001> crystallographic axes, and the first, second, and third near-neighbor surface lattice sites are outlined in the plot for clarity. (The horizontal and vertical axes of the image in Figure 5 (a) are approximately aligned along <011> directions.) The scatter in the data is due to the ±0.07 nm (0.24 *a*) uncertainty in extracting the relative pair coordinates from the image. In spite of the scatter, pair coordinates tend to fall on the 1x1 lattice sites.

Interestingly, we find no Cr pairs occupying first nearest-neighbor sites in the surface 1x1 lattice. This can be verified by comparing the Cr impurity features in Figure 5 (a) with a simulated images of Cr pairs which are shown in the inset. The horizontal and vertical axes of both the real simulated images are approximately along <110> directions. The simulated images are generated by adding Gaussian profiles for the Cr impurities with the height and width chosen to match clearly isolated features. In the simulation, a first nearest-neighbor Cr pair appears as a single feature slightly elongated along a <100> crystallographic axis. We find no oblong features oriented along <100> directions in the image.

The average occupation probability for equivalent nearest-neighbor sites is summarized by the radial pair distribution function shown in Figure 5 (c). Each data point represents a unique near-neighbor separation, and the corresponding occupation probability is determined by averaging the number of Cr-pair occurrences over all of the equivalent cells. The first data point is the zero occupation probability for first nearest-neighbor pairs. The occupation probability of second nearest-neighbor pairs is only 0.038 ± 0.007 which is $60 \pm 18\%$ of the value expected for a random distribution. At large pair separations the occupation probability saturates at the average surface Cr concentration which is 0.059 ± 0.003. The suppression of Cr near-neighbor pairs lies in stark contrast to many other surface alloy studies where clustering is observed [13]. An absence of Cr clusters could result from either kinetic effects or the presence of an effective repulsive interaction between Cr impurities.

The evolution of the Cr surface concentration with increasing Cr coverage is shown in Figure 6 for growth at 300 °C. The concentrations in the exposed regions of the substrate and in the islands are indicated by the empty and filled circles, respectively. There is an approximate linear dependence for Cr coverages less than ~0.2 ML. In this range there is no significant difference between substrate and island concentrations. The slope here is ~0.25, indicating significant interdiffusion; only one out of every 4 deposited Cr atoms remains in the surface layer. Beyond 0.2 ML, the island concentrations become difficult to quantify, but appear to increase (see Figure 3 (a)). Also at this coverage, the accumulation rate of Cr in the substrate layer begins to decrease. The Cr concentration in the exposed regions of substrate approaches approximately 9% as the Cr coverage approaches 1 ML.

Beyond a Cr deposition of 1 ML, the Cr concentration in the surface appears to continue increasing. At coverages of 2-3 ML (growth temperature range from 325 to 225°C) the images still have an alloyed appearance, but the conductance spectra suggest the presence of a significant amount of Cr in the surface layers. At these coverages, a conductance peak is still present in all spectra, but now most of the peak maxima fall at the Cr(001) surface state voltage of -0.05 V (shown in Figure 4). No conductance peak maxima are observed at the Fe(001) surface state voltage at these coverages. These data suggest that the surface is primarily Cr.

The degree of intermixing can be reduced by lowering the growth temperature. In Figure 3 we compare the alloy characteristics for growth at 180°C to growth at 300°C. The coverage is ~0.4 ML in both cases. Growth at 180°C results in a much clearer difference between the substrate and island concentrations. Compared to the 300°C condition, the substrate concentration has decreased and the island concentration appears higher. For growth even at room temperature, however, we still find alloyed Cr atoms in the substrate layer.

Often interdiffusion in surface alloys is driven by lattice mismatch effects or surface free energy differences. Because Cr and Fe are very similar these differences are small and will not provide a strong driving force for the intermixing we observe. Although the Cr/Fe bulk phase diagram shows a miscibility gap, Cr and Fe are miscible for very low and very high concentrations [14]. At 300 °C the miscibility gap extends from an alloy composition of $Cr_{0.03}Fe_{0.97}$ to a composition of $Cr_{0.97}Fe_{0.03}$. Although the equilibrium status of the system is unknown and extrapolation from bulk properties to surface properties is difficult, we

speculate that the 9% saturation of the substrate concentration may be a surface manifestation of the preferred low Cr-concentration bulk phase. We see nothing in the bulk phase diagram that would suggest the lack of Cr nearest neighbors which we observe in the surface layers.

To begin to understand the implications of the interfacial alloy on the magnetic properties, we must know the final Cr/Fe concentration profile across the interface. Our data shows that growth at 300 °C leads to significant Cr interdiffusion. Recent angle-resolved Auger electron spectroscopy experiments on this system have shown that submonolayer growth at ~300 °C results in Cr as deep as the third layer below the surface [15]. Our tunneling spectroscopy measurements show that, at least as indicated by Cr(001) and Fe(001) surface states, the surface exhibits strong Cr-like properties at Cr coverages of no more than 2 to 3 monolayers.

A diffuse rather than chemically abrupt Cr/Fe interface could be related to many of the magnetic anomalies in Cr/Fe systems. The alloying results in a spatially varying Cr concentration across the interface which will lead to an uncertainty in the position of an effective Fe/Cr interface. This could lead to the apparent reversal of the antiferromagnetic ordering and the delay of strong two-layer-period antiferromagnetic oscillations. The initial rapid change in the surface magnetization may be a consequence of the changes in Cr and neighboring Fe moments in the dilute Cr-Fe alloy [16].

We would like to thank M. D. Stiles and A. Zangwill for many helpful discussions. This work was supported in part by the Office of Naval Research.

References

[1] J. Unguris, D. T. Pierce, R. J. Celotta, and J. A. Stroscio, in *Magnetism and Structure in Systems of Reduced Dimension*, edited by R. F. C. Farrow *et al.* (Plenum, New York, 1993), p. 101; J. Unguris, R. J. Celotta, and D. T. Pierce, Phys. Rev. Lett. **67**, 140 (1991).

[2] D. T. Pierce, Joseph A. Stroscio, J. Unguris, and R. J. Celotta, Phys. Rev. B **49**, 14564 (1994).

[3] F. U. Hillebrecht, Ch. Roth, R. Jungblut, E. Kisker, and A. Bringer, Europhys. Lett. **19**, 711 (1992); P. D. Johnson, N. B. Brookes, and Y. Chang, MRS Symp. Proc. **231**, 49 (1992).

[4] B. Heinrich, Z. Celinski, J. F. Cochran, and M. From, in *Magnetism and Structure in Systems of Reduced Dimension*, edited by R. F. C. Farrow, *et al.* (Plenum, New York, 1993), p. 101.

[5] D. T. Pierce, R. J. Celotta, and J. Unguris, J. Appl. Phys. **73**, 6201 (1993); J. Unguris, R. J. Celotta, and D. T. Pierce, Phys. Rev. Lett. **69**, 1125 (1992).

[6] C. Turtur and G. Bayreuther, Phys. Rev. Lett. **72**, 1557 (1994).

[7] T. G. Walker, A. W. Pang, and H. Hopster, Phys. Rev. Lett. **69**, 1121 (1992).

[8]. A. Davies, Joseph A. Stroscio, D. T. Pierce, and R. J. Celotta, Phys. Rev. Lett. **76**, 4175 (1996).

[9] J. A. Stroscio, D. T. Pierce, and R. A. Dragoset, Phys. Rev. Lett. **70**, 3615 (1993).

[10] A. S. Arrott, B. Heinrich, and S. T. Purcell, in *Kinetics of Ordering and Growth at Surfaces*, edited by M. G. Lagally (Plenum, New York, 1990), p. 321.

[11] Joseph A. Stroscio and D. T. Pierce, J. Vac. Sci. Technol. B **12**, 1783 (1994).

[12] Joseph A. Stroscio, D. T. Pierce, A. Davies, R. J. Celotta, and M. Weinert, Phys. Rev. Lett. **75**, 2960 (1995).

[13] L. P. Nielson, F. Besenbacher, I. Stensgaard, E. Lægsgaard, C. Engdahl, P. Stoltze, K. W. Jacobson, and J. K. NØrskov, Phys. Rev. Lett. **71**, 754 (1993); H. Röder, R. Schuster, H. Brune, and K. Kern, Phys. Rev. Lett. **71**, 2086 (1993).

[14] *ASM Handbook Volume 3 Alloy Phase Diagrams*, edited by Hugh Baker, ASM International, Materials Park, Ohio, 1992.

[15] D. Venus and B. Heinrich, Phys. Rev. B **53**, R1733 (1996).

[16] V. N. Gittsovitch, V. G. Semenov, and V. M. Uzdin, J. Magn. Magn. Mater. **146**, 165 (1995).

Figure Captions

Figure 1. SEMPA measurements of Cr/Fe(001) and Fe/Cr/Fe(001) systems grown on an Fe(001) whisker at 300 °C. The top curve is the remaining secondary-electron polarization from a Cr wedge on Fe(001) after an exponential fit has been subtracted to approximately remove the contribution of the Fe substrate. The data from 0 to 1.0 ML is magnified and shown above in the inset. A SEMPA measurement of the Fe/Cr/Fe coupling is shown in the bottom of the figure.

Figure 2. STM images of 0.4 ML Cr growth on Fe(001) at 300 °C taken at a tunnel current of 0.5 nA and a sample bias of -1.1 V. (a) Large area scan showing the single atomic steps resulting from the Cr deposition. The island facets are along <100> crystallographic axes. (b) High resolution rendered image of the surface that shows the fine structure on both substrate and island levels.

Figure 3. STM images of 0.4 ML growth with the same tunneling conditions as in Figure 2. (a) Top-view image of Figure 2 (b) corresponding to growth at 300 °C. Separate grey-scales are used for the substrate (central region) and island (surrounded by a heavy black line) levels, each scale covering ~0.1 nm. (b) Similar image of growth at 180 °C.

Figure 4. Tunneling conductance spectra. The dashed-line curves are representative of

spectra taken on clean Cr(001) and Fe(001) surfaces. The solid-line curves are examples of spectra on the Cr/Fe alloyed surface. A schematic of the surface configuration for growth at 300 °C is shown at the bottom of the figure.

Figure 5. Evaluation of the spatial correlation of the alloyed Cr impurities. (a) High-resolution STM image of a substrate-level region showing the alloyed Cr atoms. The inset shows simulated images of near-neighbor Cr impurities to be compared with the features in the image. The vertical and horizontal edges of both the real and simulated images are approximately aligned with <110> crystallographic axes of the Fe(001) substrate. (b) Two-dimensional pair distribution plot of the relative Cr-pair coordinates from the image in part a. The axes are along <100> directions, which is rotated relative to the orientation in part a. The area of each symbol is proportional to the number of Cr pairs with relative coordinates $(x \pm \delta)_{[100]}$ and $(y \pm \delta)_{[010]}$, using a bin size of $\delta = a/32$ where a = 0.288 nm is the in-plane lattice constant. Unit cells corresponding to first, second and third surface near-neighbors are indicated in the figure. (c) Plot of the average pair occupation probability for equivalent surface near-neighbor sites as determined from the data in part b. The horizontal axis is in units of the lattice constant which is 0.288 nm.

Figure 6. Cr coverage dependence of the alloy Cr concentration. The empty (filled) circles represent the concentration on the substrate (island) level.

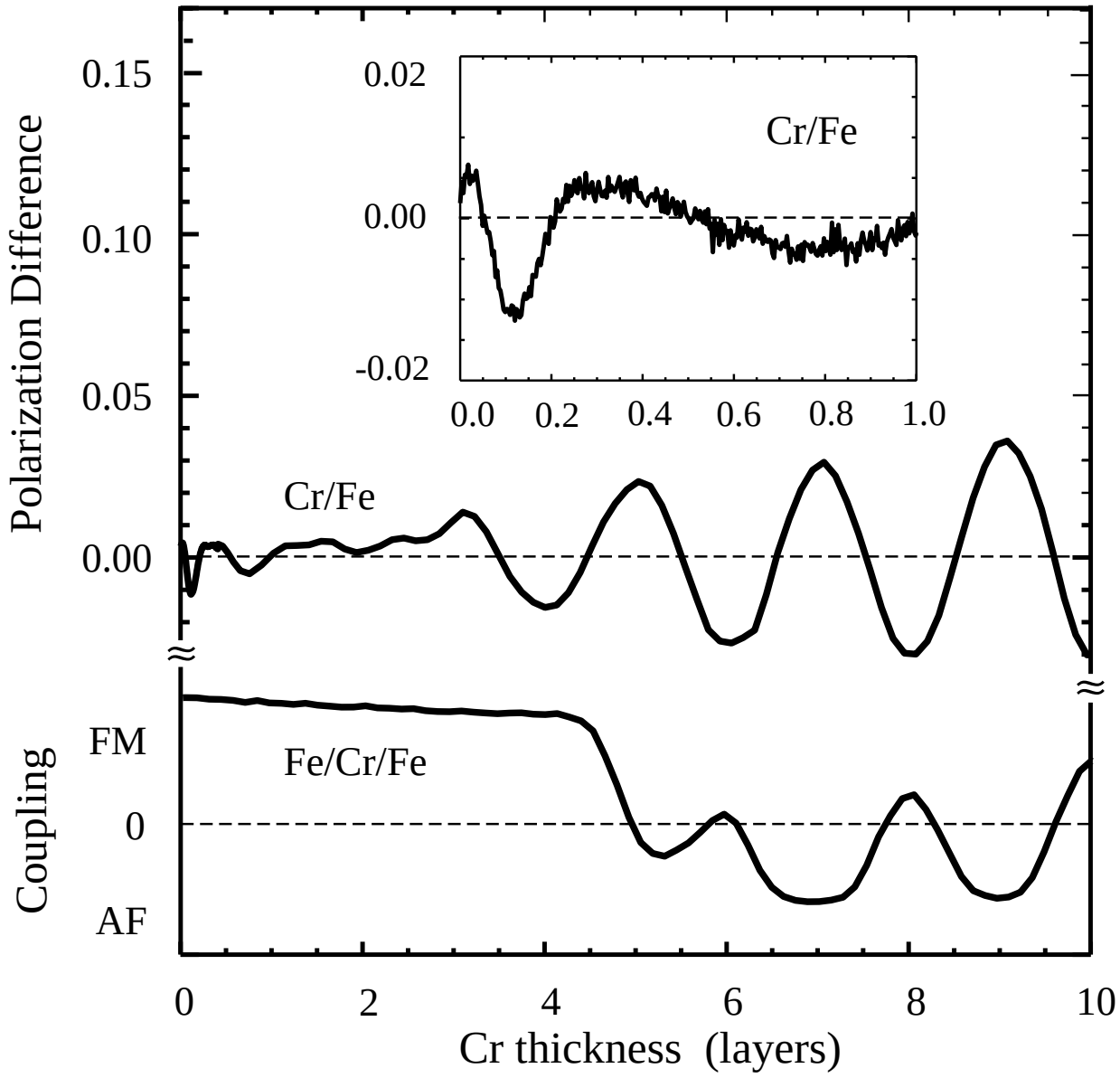
Polarization Difference
0.15
0.10
0.05
0.00
0.02
0.00
-0.02
0.0
0.2
0.4
0.6
0.8
1.0
Cr/Fe
Cr/Fe
Coupling
FM
0
AF
Fe/Cr/Fe
0
2
4
6
8
10
Cr thickness (layers)

Figure 1

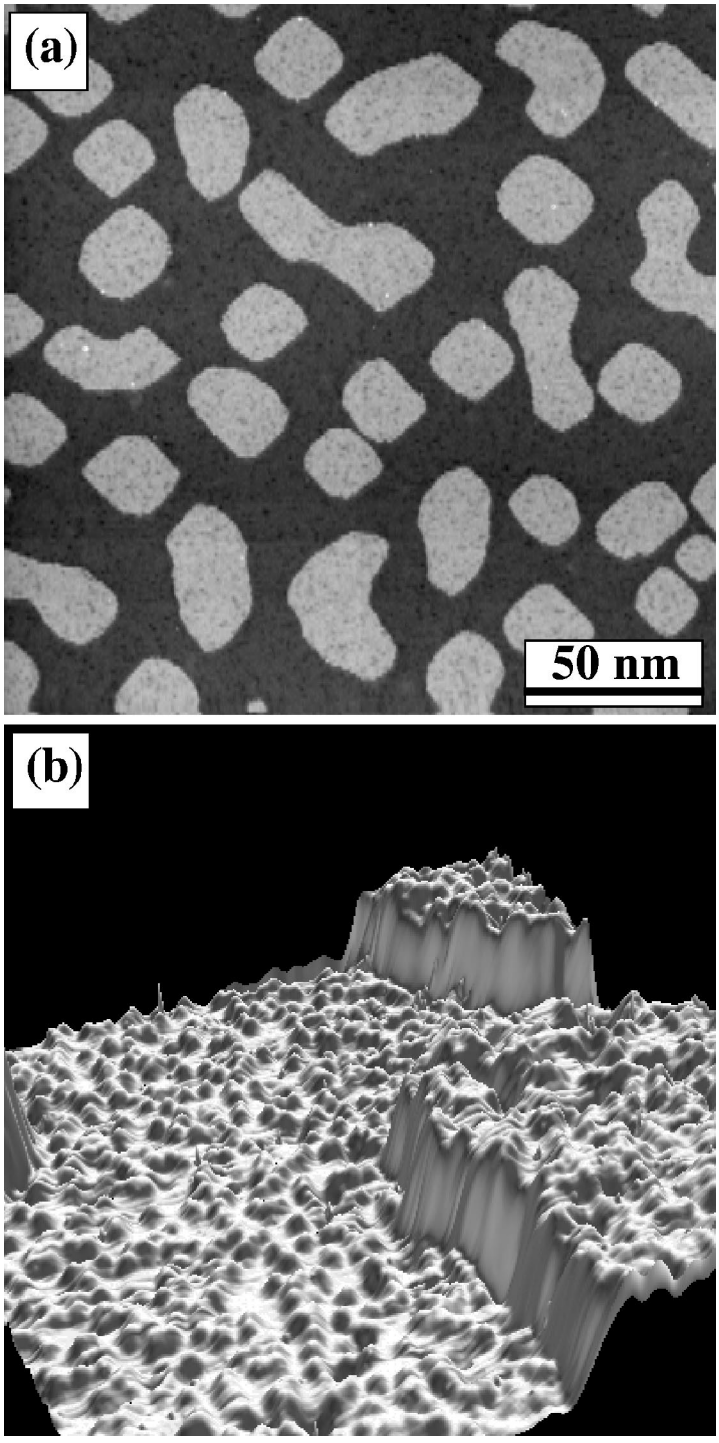

Figure 2

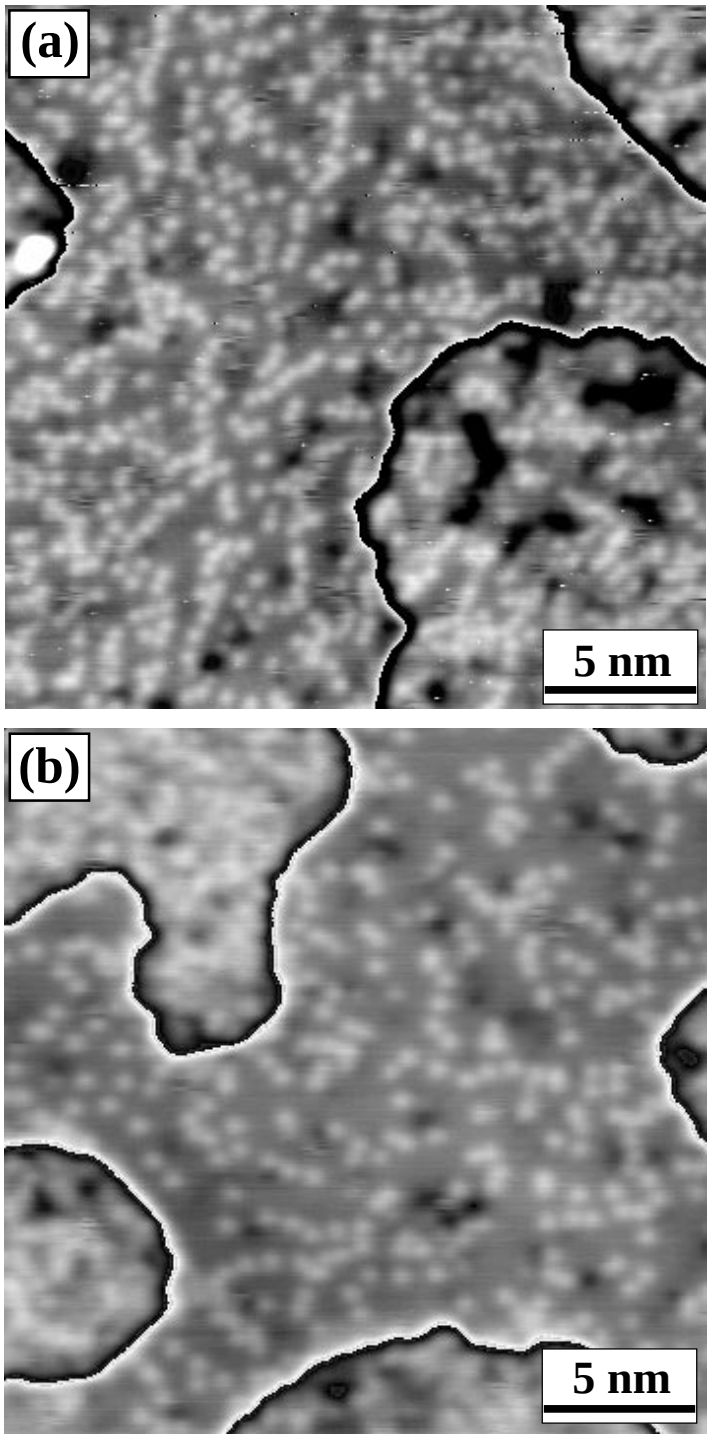

Figure 3

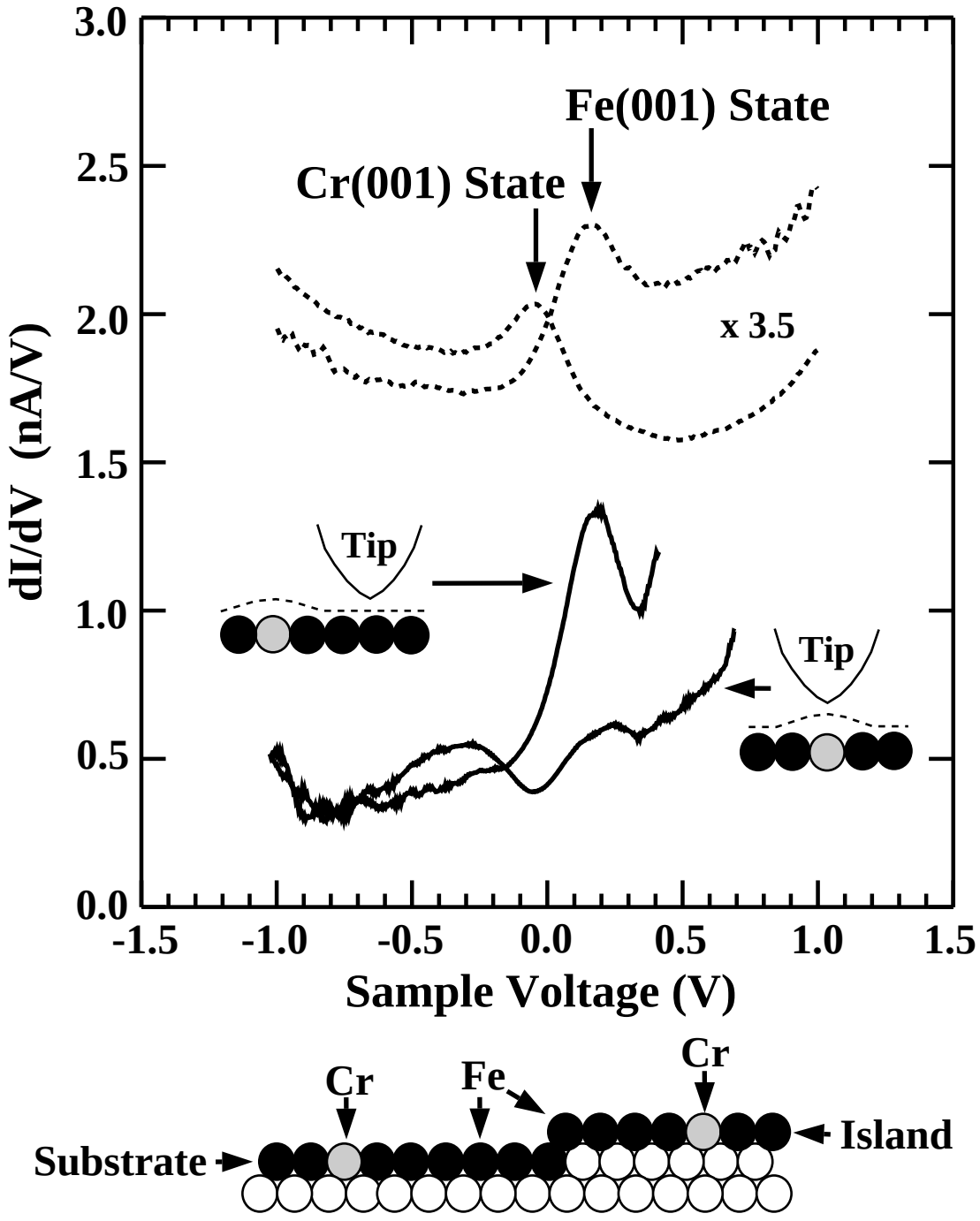
3.0
2.5
2.0
1.5
1.0
0.5
0.0
dI/dV (nA/V)
Fe(001) State
Cr(001) State
x 3.5
Tip
Tip
-1.5
-1.0
-0.5
0.0
0.5
1.0
1.5
Sample Voltage (V)
Cr
Fe
Cr
Substrate
Island

Figure 4

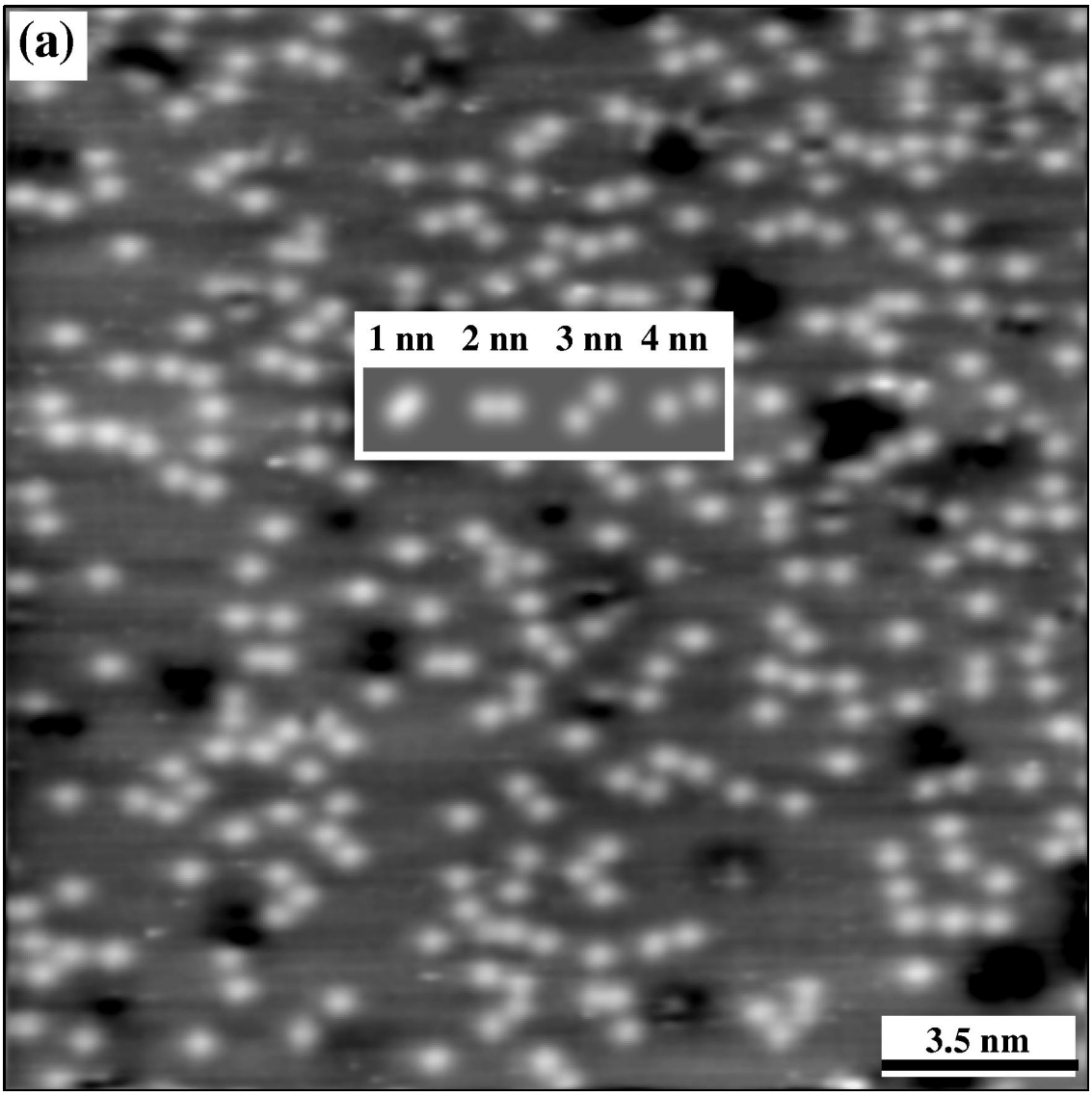

Figure 5a

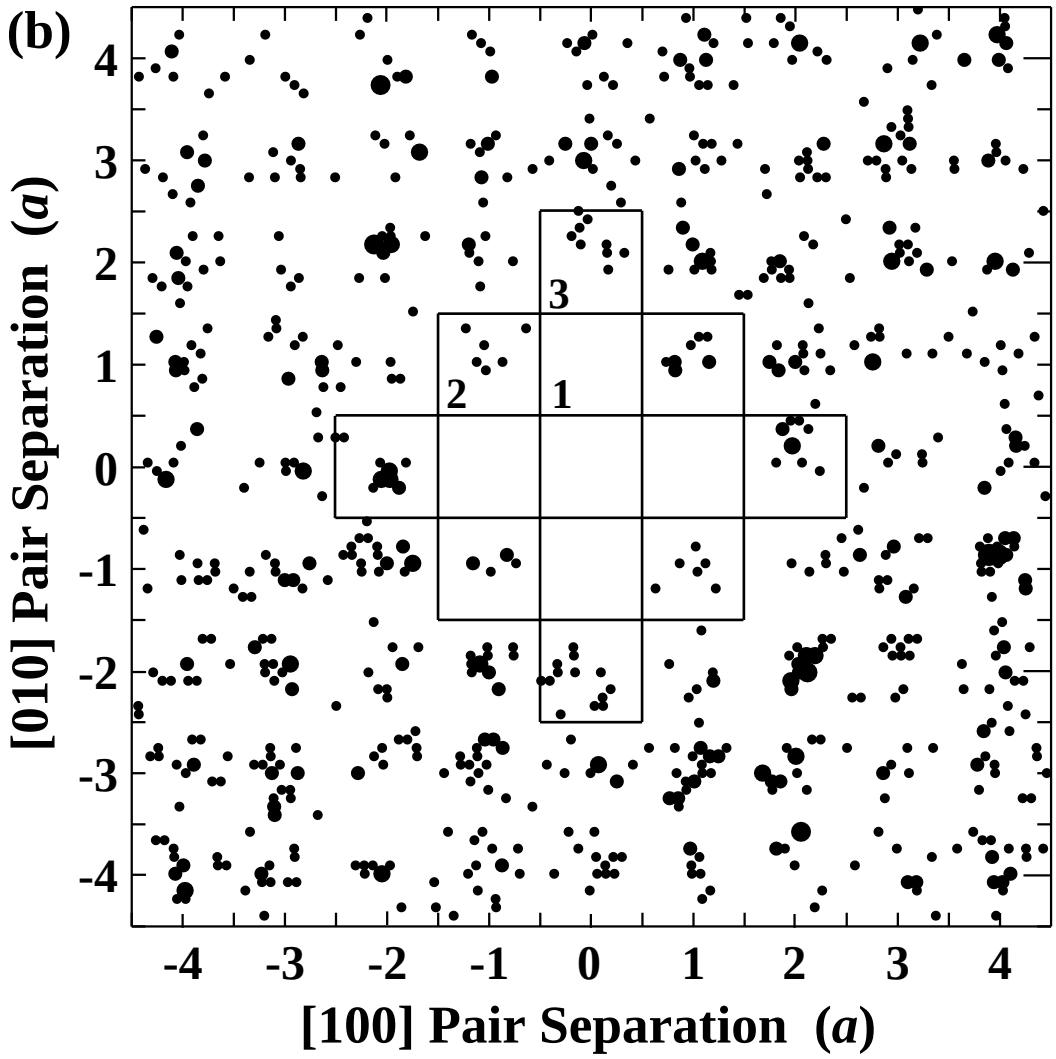
(b)
[010] Pair Separation (a)
[100] Pair Separation (a)
4
3
2
1
0
-1
-2
-3
-4
-4
-3
-2
-1
0
1
2
3
4
3
2
1

Figure 5b

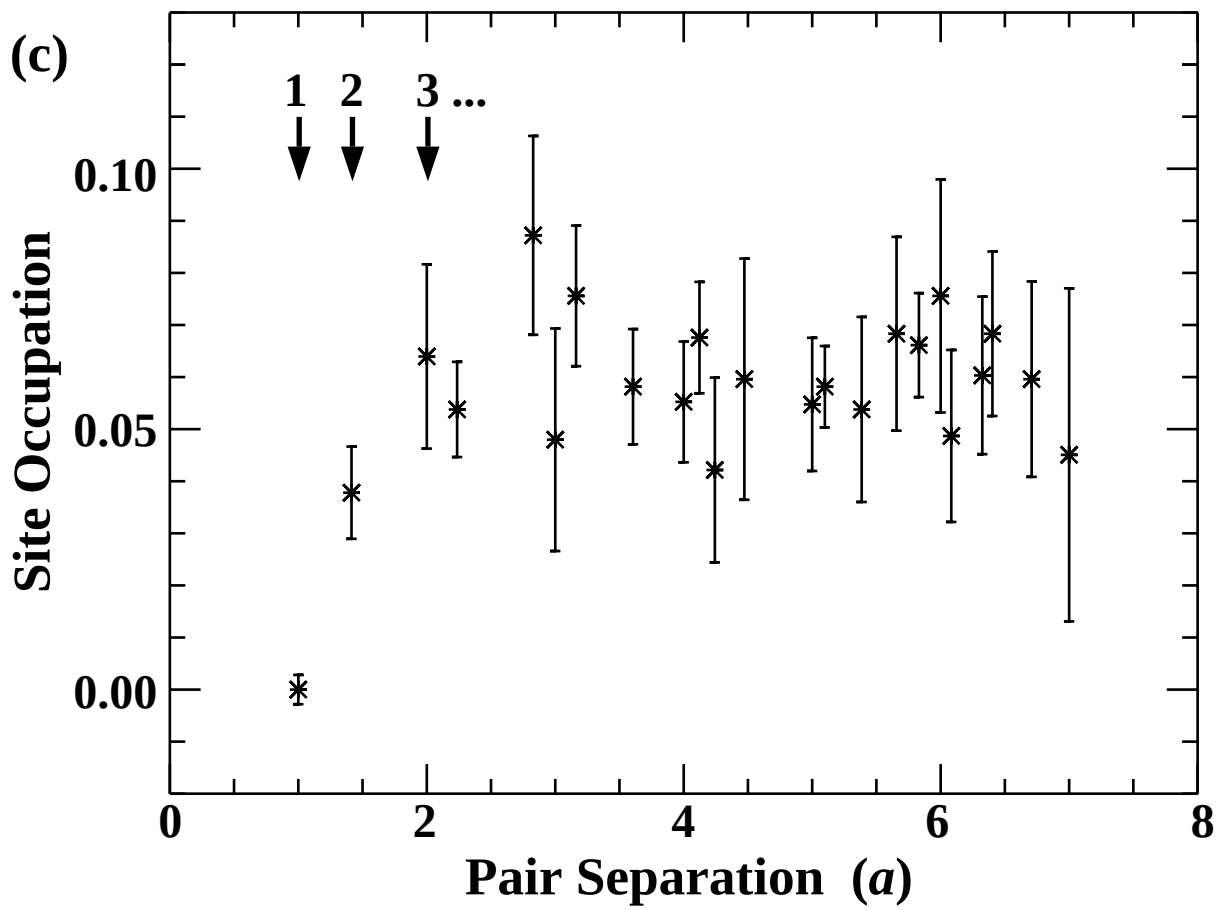

Figure 5c

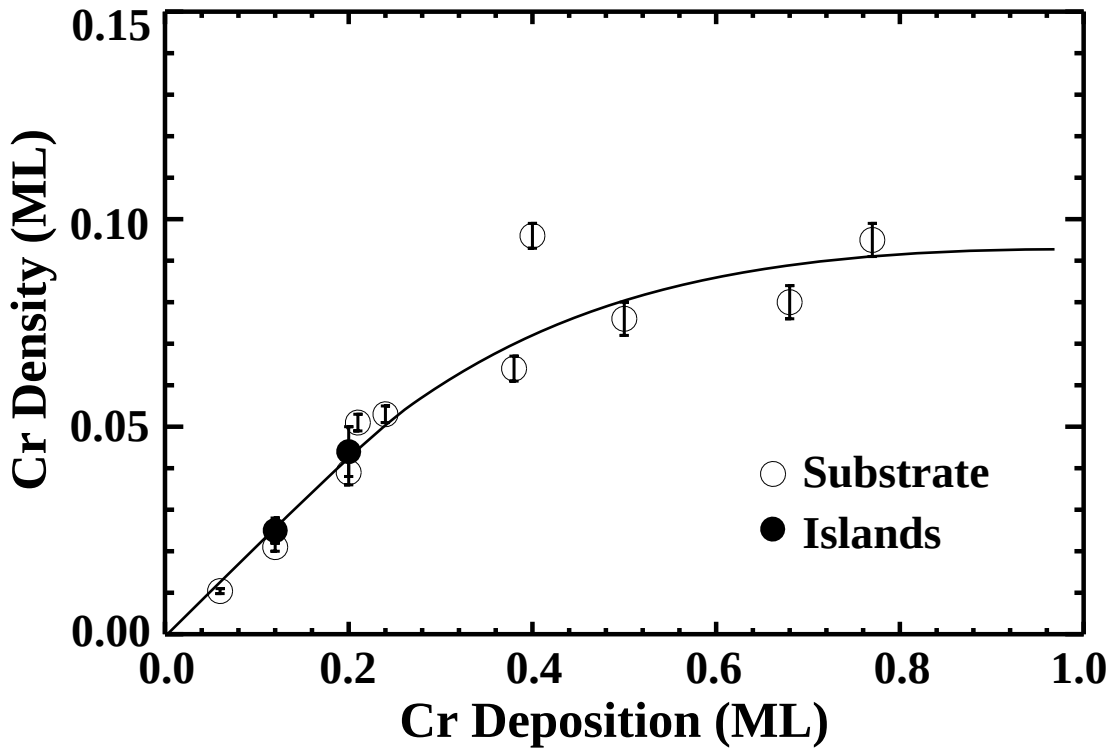
0.15
0.10
0.05
0.00
Cr Density (ML)
0.0
0.2
0.4
0.6
0.8
1.0
Cr Deposition (ML)
Substrate
Islands

Figure 6